

Observation of a shape resonance in the $a^3\Sigma_u^+$ state of ${}^7\text{Li}_2$

R. Côté and A. Dalgarno

Institute for Theoretical Atomic and Molecular Physics (ITAMP), Harvard-Smithsonian Center for Astrophysics, 60 Garden Street, Cambridge, Massachusetts 02138

A. M. Lyyra

Department of Physics, Temple University, Philadelphia, Pennsylvania 19122

Li Li

Department of Modern Applied Physics, Tsinghua University, Beijing 100084, China

(Received 17 March 1999; revised manuscript received 8 June 1999)

Using the most accurate potential curves available for the $a^3\Sigma_u^+$ and $X^1\Sigma_g^+$ states of lithium molecules, we compute the positions of shape resonances. We also calculate the deexcitation probability from a bound level v' with rotational number N' to the continuum of the lower state, and conclude that a shape resonance should be measurable for the transition $2^3\Pi_g \rightarrow a^3\Sigma_u^+$. Such a shape resonance has been identified from the spectra of the transition from the $v'=2, N'=4$ level of $2^3\Pi_g$ into the $N''=4$ continuum of $a^3\Sigma_u^+$. Its position is in good agreement with the theoretical prediction. [S1050-2947(99)09909-6]

PACS number(s): 33.20.Vq, 33.50.Dq, 33.70.Ca, 34.20.Cf

I. INTRODUCTION

In spectroscopic experiments on the molecule ${}^7\text{Li}_2$, an array of emission lines arising in transitions from the $2^2\Pi_g$ state to the $a^3\Sigma_u^+$ state has been detected and analyzed [1,2]. In addition to the series of lines originating from the $v'=2, N'=4$ rovibrational level, there is an unidentified feature in the spectrum close to the transition to the last bound level $v''=9, N''=4$ of the lower electronic state [3]. We argue here that the feature can be attributed to a transition into a g -wave shape resonance lying in the vibrational continuum of the $a^3\Sigma_u^+$ state. Similar shape resonances occur in the ground $X^1\Sigma_g^+$ state and the singlet and triplet states of the isotopic variants ${}^6\text{Li}_2$ and ${}^6\text{Li}{}^7\text{Li}$. We predict their positions and widths.

Using photoassociation techniques, shape resonances have been measured for collisions between ${}^{85}\text{Rb}$ atoms [4], and ${}^{87}\text{Rb}$ atoms [5] in the ultracold temperature regime. These are resonances associated with quasibound diatomic levels trapped behind a centrifugal barrier, and are important because the collision energies of ultracold atoms are typically lower than the centrifugal barrier even for the lowest partial waves. The position and width of a shape resonance is very sensitive to the details of the potential, and knowledge of these quantities may lead to even more accurate potential curves. In addition to improving the accuracy of the scattering lengths, shape resonances may be expected to shed new light on the elastic and inelastic interactions of cold atoms. The important role of elastic shape resonances in inelastic scattering has long been recognized [6]. Shape resonances may lead to a new kind of spectroscopy of states inside the centrifugal barrier [7] with a tunneling lifetime long enough for inelastic interactions to occur due to weak interaction terms that are difficult to study otherwise.

II. EXPERIMENT

The experimental details have been described in Ref. [1]. Lithium vapor was generated in a heatpipe oven. Perturba-

tion facilitated optical-optical double resonance spectroscopy has been used to access the $2^3\Pi_g$ state of ${}^7\text{Li}_2$ via $2^3\Pi_g \leftarrow (A^1\Sigma_u^+ \sim b^3\Pi_u) \leftarrow X^1\Sigma_g^+$ excitation using two single-mode tunable dye lasers. The $A^1\Sigma_u^+ \sim b^3\Pi_u$ mixed levels provide gateways through which the triplet manifold can be accessed. When the two laser frequencies were held fixed to excite a $2^3\Pi_g v', N' \leftarrow A^1\Sigma_u^+ \sim b^3\Pi_u \leftarrow X^1\Sigma_g^+$ transition, $2^3\Pi_g v', N' \rightarrow a^3\Sigma_u^+$ fluorescence was dispersed by a Spex 1404 0.75 M double-grating monochromator.

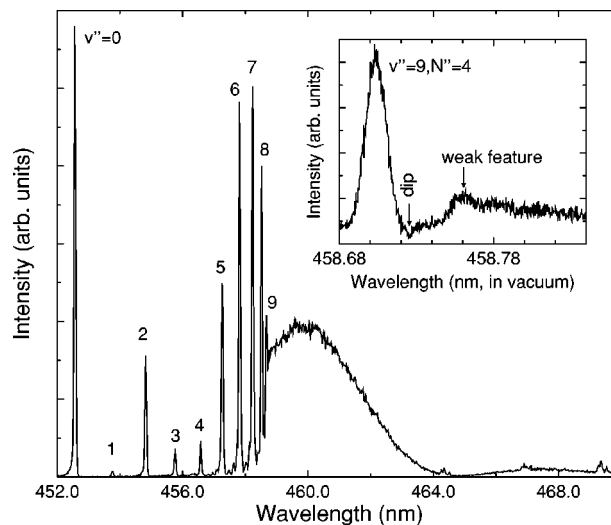


FIG. 1. Resolved fluorescence spectrum of $2^3\Pi_g v'=2, N'=4 \rightarrow a^3\Sigma_u^+$ state. The ten sharp lines are the $2^3\Pi_g v'=2, N'=4 \rightarrow a^3\Sigma_u^+ v''=0-9, N''=4 Q_3$ lines. The upper right spectrum is an enlargement of the threshold region with a high-resolution scan (monochromator slit, $40 \mu\text{m}$). A weak feature appears at $2.5 \pm 0.2 \text{ cm}^{-1}$ from the $v''=9$ level. The dip was caused by insertion of the mechanical chopper in one of the laser beams momentarily to facilitate checking of the optical-optical double resonance signal level against possible laser-frequency drift.

TABLE I. RKR data generated from the molecular constants of Ref. [1]. Here, the equilibrium distance is $R_e = 3.842\,239\text{ \AA}$.

v	G_v^a (cm^{-1})	R_{\min} (\AA)	R_{\max} (\AA)
0	94.2493	3.6224	4.0750
1	280.5636	3.4678	4.2558
2	464.6401	3.3643	4.3866
3	646.5657	3.2817	4.4973
4	826.4178	3.2115	4.5965
5	1004.2656	3.1497	4.6880
6	1180.1703	3.0941	4.7742
7	1354.1864	3.0434	4.8562
8	1526.3618	2.9966	4.9352
9	1696.7388	2.9531	5.0116
10	1865.3544	2.9124	5.0860
11	2032.2412	2.8742	5.1588
12	2197.4275	2.8380	5.2302
13	2360.9381	2.8038	5.3005
14	2522.7946	2.7713	5.3698
15	2683.0156	2.7403	5.4384
16	2841.6177	2.7107	5.5064
17	2998.6151	2.6824	5.5738
18	3154.0201	2.6553	5.6409
19	3307.8437	2.6294	5.7076
20	3460.0955	2.6044	5.7741
21	3610.7837	2.5804	5.8404
22	3759.9157	2.5574	5.9067
23	3907.4980	2.5352	5.9729
24	4053.5359	2.5138	6.0391
25	4198.0344	2.4931	6.1054
26	4340.9971	2.4732	6.1718
27	4482.4271	2.4540	6.2384
28	4622.3264	2.4355	6.3052
29	4760.6958	2.4176	6.3723
30	4897.5350	2.4003	6.4397
31	5032.8423	2.3835	6.5074
32	5166.6140	2.3674	6.5755
33	5298.8449	2.3518	6.6441
34	5429.5273	2.3366	6.7131
35	5558.6508	2.3220	6.7827
36	5686.2023	2.3079	6.8529
37	5812.1651	2.2942	6.9238
38	5936.5188	2.2809	6.9955
39	6059.2385	2.2680	7.0680
40	6180.2947	2.2555	7.1414
41	6299.6522	2.2433	7.2158

^aThe term $Y_{00} = -0.223\,2\text{ cm}^{-1}$ is included.

Three pairs of $A\ ^1\Sigma_u^+ \sim b\ ^3\Pi_u$ mixed levels [$A\ ^1\Sigma_u^+$ $v=13, J=4, 7, 11$ with $b\ ^3\Pi_u$ $v=19, N=5$ ($F_3, J=4e$), 7 ($F_2, J=7e$), 10 ($F_1, J=11e$), respectively] have been identified in $^7\text{Li}_2$. When the $2\ ^3\Pi_g$ $v'=2, N'=4, F_3, J'=3e$ level is excited via the $b\ ^3\Pi_u$ $N=5, F_3, J=4e$ intermediate level, the upper $2\ ^3\Pi_g$ $N'=4, F_3, J'=3e$ level can fluoresce to the $a\ ^3\Sigma_u^+$ $N''=4$ ($F_3, J''=3f$) and 2 ($F_1, J''=3f$) lower levels according to the selection rules. The $\Delta N \neq \Delta J, N'=4 \rightarrow N''=2$ $^5Q_{13}$ lines are much weaker than the $\Delta N = \Delta J,$

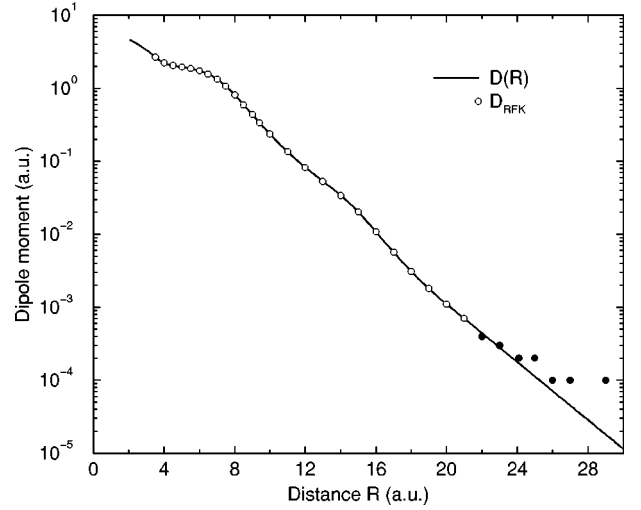


FIG. 2. The dipole moment for the $2\ ^3\Pi_g \rightarrow a\ ^3\Sigma_u^+$ transition. It should tend to zero rapidly at large R . The *ab initio* values indicated by \bullet were not used.

$N'=4 \rightarrow N''=4$ Q_3 lines such that only $N'=4 \rightarrow N''=4$ Q_3 lines (and collision-induced $N'=N''$ Q_3 lines) have been observed in our resolved fluorescence spectra. Figure 1 is the $2\ ^3\Pi_g$ $v'=2, N'=4 \rightarrow a\ ^3\Sigma_u^+$ resolved fluorescence spectrum with a monochromator slit of $200\ \mu\text{m}$. The ten sharp lines in the spectrum are transitions into the $a\ ^3\Sigma_u^+$ $v''=0-9$ levels. The upper spectrum is an enlargement of the threshold region with a high resolution scan (monochromator slit, $40\ \mu\text{m}$). A weak feature appears at about $2.5 \pm 0.2\text{ cm}^{-1}$ from the spectral line corresponding to $v''=9$.

III. THEORY

The probability of spontaneous emission from a bound vibrational level v' of the initial electronic state of Li_2 into the vibrational continuum of the lower state, in a transition in which there is no change in the rotational quantum number N' , is given by [8,9]

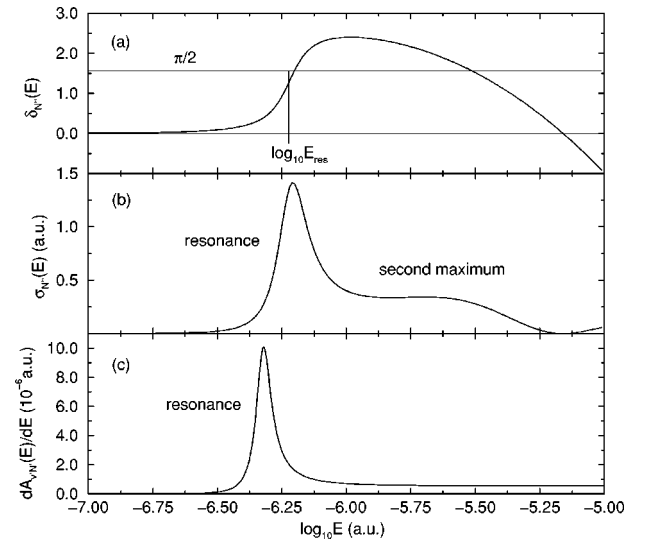


FIG. 3. Elastic phase shift $\delta_{N''}(E)$ (a) and elastic cross section $\sigma_{N''}(E)$ (b) for $N''=4$ in the $a\ ^3\Sigma_u^+$ state. In (c), we show $dA_{v',N''}(E)/dE$ for $v'=2, N'=4$.

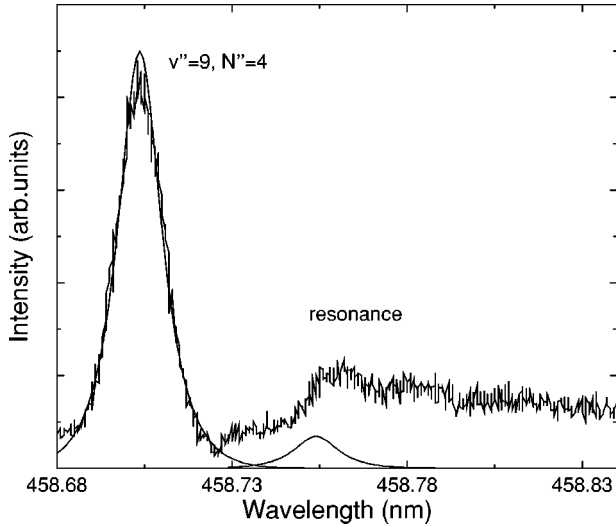


FIG. 4. Theoretical profiles for the last level $v''=9$ and the resonance. The lines are a product of a Lorentzian and a Gaussian with a width corresponding to the experimental resolution of 0.162 Å. If the background signal in the continuum is removed, the theoretical and experimental location and relative intensities come into good agreement.

$$\frac{dA_{v'N'}(E)}{dE} = \frac{4}{3} \frac{e^2 \omega_{v'}^3}{\hbar c^3} |D_{v'N'}(E)|^2, \quad (1)$$

where $\omega_{v'} = (E_{v'N'} - E)/\hbar$ is the frequency of the emitted photon, $E_{v'N'}$ is the energy of the initial level, E is the energy of the relative motion in the final state, and $D_{v'N'}(E)$ is the transition dipole matrix element. The transition dipole matrix element is given by

$$D_{v'N'}(E) = \int_0^\infty dR u_{v',N'}^*(R) D(R) u_{E,N'}(R), \quad (2)$$

where $u_{v',N'}(R)$ is the nuclear wave function of the initial vibrational level, $u_{E,N'}(R)$ is the energy normalized nuclear wave function in the final vibrational continuum, and $D(R)$ is the electronic transition moment connecting the two electronic states. The bound-bound spontaneous emission probability is given by

$$A_{v'N' \rightarrow v''N''} = \frac{4}{3} \frac{e^2 \omega^3}{\hbar c^3} |D_{v'N'}^{v''N''}|^2, \quad (3)$$

where $\omega = (E_{v'N'} - E_{v''N''})/\hbar$ and the dipole matrix element is $D_{v'N'}^{v''N''} = \int_0^\infty dR u_{v',N'}^*(R) D(R) u_{v'',N''}(R)$ [9].

TABLE II. Turning points defined by the shape resonance in the $N''=4$ partial wave of the $a^3\Sigma_u^+$ state of ${}^7\text{Li}_2$ and inner turning points R_{\min} for the four lowest levels of the $2^3\Pi_g$ state of ${}^7\text{Li}_2$ for $N'=4$, and outer turning points R_{\max} for the four highest levels.

$\log_{10} E_{\text{res}}$ (a.u.)	R_1 (a_0)	R_2 (a_0)	R_3 (a_0)	v'	R_{\min} (a_0)	v'	R_{\max} (a_0)
-6.23	6.3826	37.521	45.90	0	6.848	70	29.15
				1	6.555	71	32.65
				2	6.360	72	37.89
				3	6.204	73	47.15

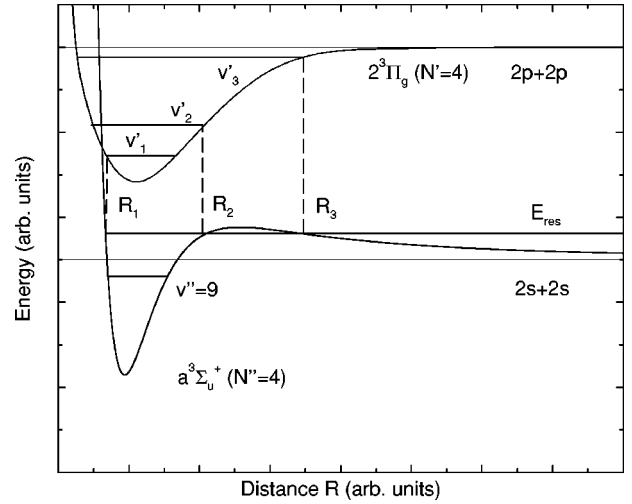


FIG. 5. Sketch of the potential curves for the Q -branch transitions with $N'=4$ from bound levels of $2^3\Pi_g$ to $a^3\Sigma_u^+$. The centrifugal barrier in the lower state gives rise to a shape resonance located above the last bound level $v'=9$ at E_{res} , and defines three classical turning points R_1, R_2 , and R_3 . The bound levels with the largest Franck-Condon overlap are indicated by v'_1, v'_2 , and v'_3 .

In the Born-Oppenheimer approximation, the radial wave function of the excited bound state $u_{v',N'}(R)$ is the well-behaved normalized solution of the equation

$$\left(\frac{d^2}{dR^2} + K^2 - \frac{2\mu}{\hbar^2} V_x(R) - \frac{N'(N'+1)}{R^2} \right) u_{v',N'}(R) = 0, \quad (4)$$

where $E_{v',N'} = \hbar^2 K^2 / 2\mu$, μ is the reduced mass, and $V_x(R)$ is the excited interatomic potential. The lower-state eigenfunction $u_{E,N''}(R)$ is the regular solution of the partial wave equation

$$\left(\frac{d^2}{dR^2} + k^2 - \frac{2\mu}{\hbar^2} V_g(R) - \frac{N''(N''+1)}{R^2} \right) u_{E,N''}(R) = 0, \quad (5)$$

where $V_g(R)$ is the lower-state interatomic potential, $E = \hbar^2 k^2 / 2\mu$, and k is the wave number. The radial wave function is normalized with respect to the energy, and $u_{E,N''}(R)$ has the asymptotic form

$$u_{E,N''}(R) \sim \left(\frac{2\mu}{\pi \hbar^2 k} \right)^{1/2} \sin \left[kR - \frac{N''\pi}{2} + \delta_{N''}(k) \right], \quad (6)$$

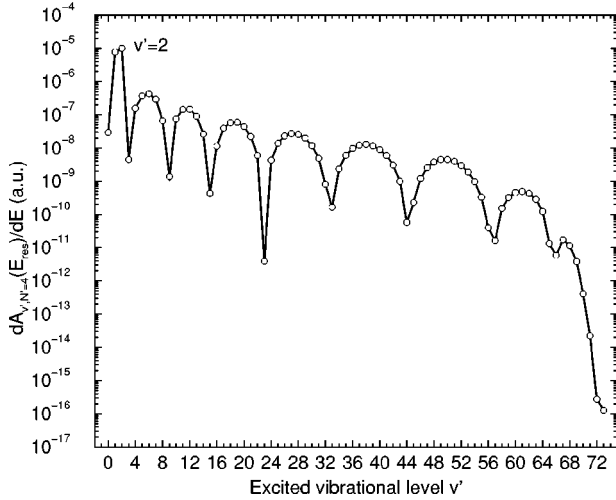


FIG. 6. The probability of spontaneous emission $dA_{v',N'=4}(E_{\text{res}})/dE$ for the various levels v' of the $2^3\Pi_g$ state for the $2^3\Pi_g \rightarrow a^3\Sigma_u^+$ transition with $N'=N''=4$. The resonance energy is $E_{\text{res}} = 10^{-6.32}$ a.u.

where $\delta_{N''}(k)$ is the elastic scattering phase shift. The elastic cross section for a particular partial wave N'' is

$$\sigma_{N''}(E) = \frac{4\pi}{k^2} (2N'' + 1) \sin^2[\delta_{N''}(k)]. \quad (7)$$

If shape resonances occur, their position E_{res} and width Γ may be determined from

$$\Gamma = 2 \left(\frac{\partial}{\partial E} \delta_{N''}(E) \right)_{E=E_{\text{res}}}^{-1} \quad (8)$$

with the resonance lifetime given by $\tau = \hbar/\Gamma$.

IV. POTENTIALS AND DIPOLE MOMENT

For the lower $a^3\Sigma_u^+$ state, we adopt the potential described in Ref. [10]. To construct the excited-state potential for $2^3\Pi_g$, we used RKR (Rydberg-Klein-Rees) data supplemented by *ab initio* values. From the molecular constants in Ref. [1], we generated RKR data for levels up to 41 (see Table I). *Ab initio* data from Ref. [1] for $R = 3.75a_0$ were used to complete the short-range section of the potential. For $R < 3.75a_0$, the short-range form is given by

$$V(R) = A \exp(-BR) \quad \text{for } R \leq 3.75a_0 \quad (9)$$

with

$$A = V(R) \exp(BR) \Big|_{3.75} \quad \text{and} \quad B = - \left. \frac{\partial \ln V(R)}{\partial R} \right|_{3.75}. \quad (10)$$

At large distance, we extended the potential with the long-range form

$$V(R) \approx - \frac{C_6}{R^6} - \frac{C_8}{R^8}. \quad (11)$$

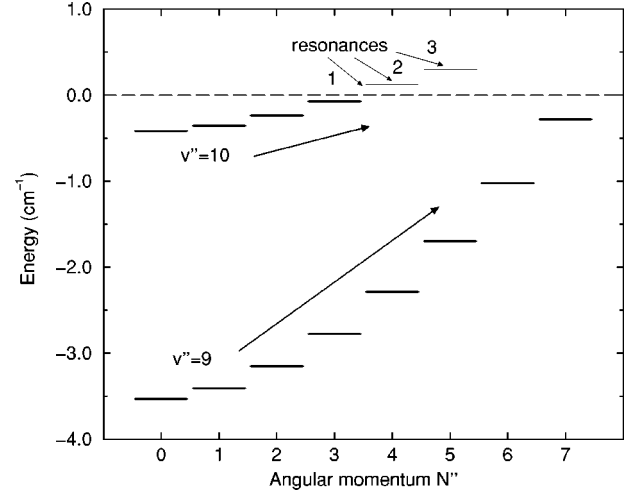


FIG. 7. Rotational energy levels of the $v''=9$ and 10 vibrational levels of the $a^3\Sigma_u^+$ state of $^7\text{Li}_2$. Shape resonances occur for $N''=4$ and 5 . For $N''=4$, we show the location of the resonance both in $dA_{v',N'}(E)/dE$ (labeled 1) at $E_{\text{res}} = 10^{-6.32}$ a.u., and in the elastic cross section $\sigma_{N''}(E)$ (labeled 2) at $E_{\text{res}} = 10^{-6.23}$ a.u. For $N''=5$, we show only the location of the resonance in the elastic cross section (labeled 3) at $E_{\text{res}} = 10^{-5.87}$ a.u. (see also Table III).

We take $C_6 = 31\,965$ a.u., and $C_8 = 1\,006\,900$ a.u. from Marinescu [11]. Finally, we estimated the value of the dissociation energy $D_e(\Pi)$ for the $2^3\Pi_g$ state using the value of $T_e = 29\,844.654\,01$ cm^{-1} [12], $D_e(X) = 8\,516.75$ cm^{-1} of the $X^1\Sigma_g^+$ state [10], and the energy difference $\Delta = 2 \times 14\,903.887$ cm^{-1} between the $2s+2s$ and $2p+2p$ limit:

$$D_e(\Pi) = \Delta + D_e(X) - T_e = 8\,479.870 \text{ cm}^{-1}, \quad (12)$$

which is larger than the value $8\,380$ cm^{-1} proposed in Ref. [14].

We used the values D_{RFK} of the electronic transition moment $D(R)$ calculated by Ratcliff, Fish, and Konowalow [15] for distances ranging from 3.5 to $21.0a_0$. The accuracy of the data is limited for larger R and we continued the dipole moment for $R > 21.0a_0$ by an exponential

$$D(R) = A_D \exp(-B_D R) \quad \text{for } R \geq 21.0a_0 \quad (13)$$

where $B_D = -d \ln D_{\text{RFK}}(R) / dR \Big|_{21.0} = 0.4\,568$ and $A_D = D_{\text{RFK}}(R) \exp(B_D R) \Big|_{21.0} = 10.268$. At very large R , $D(R)$ varies as R^{-7} but the long-range dipole makes little contribution to the dipole matrix. For $R < 3.5a_0$, we use the linear form $D(R) = D(3.5) + (R - 3.5) dD/dR \Big|_{3.5}$, where $dD/dR \Big|_{3.5} = -1.348\,7$. The full curve with the original data points from Ref. [15] is shown in Fig. 2.

V. RESULTS

We computed the elastic phase shift and elastic cross section for partial waves with angular momentum N'' less or equal to 7 for the $a^3\Sigma_u^+$ potential of $^7\text{Li}_2$. We found a shape resonance for $N''=4$ at an energy E_{res} of $10^{-6.23}$ a.u. or 0.13 cm^{-1} above the dissociation threshold. We illustrate the phase shift and the cross section in Figs. 3(a) and 3(b), respectively. The calculated radiative intensity distribution for the transition $v'=2, N'=4$ to $E, N''=4$ is shown in Fig. 3(c).

TABLE III. Shape resonances for the triplet $a^3\Sigma_u^+$ potentials. Here, v''_{\max} corresponds to the highest vibrational level with $N''=0$. For ${}^7\text{Li}_2$, the resonances arise from $v''=10$ moving into the continuum [see also Fig. 7]. For ${}^6\text{Li}_2$, the first resonance ($N''=4$) is due to the appearance of a new quasibound level ($v''=10$); the next two correspond to $v''=9$ being lifted into the continuum. For ${}^6\text{Li}-{}^7\text{Li}$, the $N''=2$ resonance is due to $v''=10$ being lifted into the continuum, and the next two resonances are due to $v''=9$ moving into the continuum.

N''	v''	$\log_{10} E_{\text{res}}$ (a.u.)	Γ (a.u.)	τ (s)
${}^7\text{Li}_2$: $D_e=333.78 \text{ cm}^{-1}$, $v''_{\max}=10$				
4	10	-6.23	2.01×10^{-7}	1.20×10^{-10}
5	10	-5.87	1.07×10^{-6}	2.25×10^{-11}
${}^6\text{Li}_2$: $D_e=333.74 \text{ cm}^{-1}$, $v''_{\max}=9$				
4	10	-6.47	1.35×10^{-8}	1.79×10^{-9}
5	9	-5.82	5.72×10^{-7}	4.23×10^{-11}
6	9	-5.55	2.17×10^{-6}	1.11×10^{-11}
${}^6\text{Li}-{}^7\text{Li}$: $D_e=333.76 \text{ cm}^{-1}$, $v''_{\max}=10$				
2	10	-6.90	1.50×10^{-7}	1.62×10^{-10}
6	9	-5.86	5.82×10^{-8}	4.15×10^{-10}
7	9	-5.47	8.37×10^{-7}	3.00×10^{-11}

Because of the rapid decrease with R of the dipole moment, the energy at which the intensity is maximal lies below the resonance energy at $E=10^{-6.32}$ a.u. and the second maximum apparent in the elastic cross section in Fig. 3(b) is suppressed. The width is also smaller: 8.48×10^{-8} a.u. compared to 2.01×10^{-7} a.u. (see also Table III). The shift in energy is 0.02 cm^{-1} placing the feature at 0.11 cm^{-1} above threshold. The last bound level $v''=9, N''=4$ is located 2.28 cm^{-1} below threshold; hence, the feature is located at 2.39 cm^{-1} above the last bound level of the $a^3\Sigma_u^+$ state of ${}^7\text{Li}_2$.

We have computed the bound-bound spontaneous transition probability between the level $v'=2, N'=4$ of the upper state and the highest lying level $v''=9, N''=4$ of the lower state. We obtained $A(v'=2, N'=4 \rightarrow v''=9, N''=4) = 1.12 \times 10^{-11}$ a.u. (or $4.63 \times 10^5 \text{ s}^{-1}$). To compare with the reso-

nance feature, we multiply the resonance transition probability $dA_{v'=2, N'=4}(E_{\text{res}})/dE = 1.01 \times 10^{-5}$ a.u. by its width $\Gamma_{\text{res}} = 8.48 \times 10^{-8}$ a.u. to get $A(v'=2, N'=4 \rightarrow \text{continuum}) \approx 8.56 \times 10^{-13}$ a.u. (or $3.54 \times 10^4 \text{ s}^{-1}$). We expect the fluorescence signal of the shape resonance to be 0.076 times the intensity of the line into the last bound level $v''=9, N''=4$.

We have convolved the calculated values of the transition probability by a Voigt profile formed by a Lorentzian and a Gaussian with widths set to the instrumental value of 0.162 \AA (or 3.5×10^{-6} a.u.) [3]. They are presented in Fig. 4, where they are compared with the measured features. The theoretical and experimental profiles match closely.

Similar features will be present in association with discrete transitions from other vibrational levels v' of the $2^3\Pi_g$ state. The largest values will occur when the Franck-Condon

TABLE IV. Shape resonances for the singlet $X^1\Sigma_g^+$ potentials. Here, v''_{\max} corresponds to the highest vibrational level with $N''=0$. For ${}^7\text{Li}_2$, the first two resonances arise from $v''=41$ moving into the continuum, and the third one ($N''=7$) is due to $v''=40$ being lifted into the continuum. For ${}^6\text{Li}_2$, the first resonance ($N''=2$) is due to the highest level $v''=38$ being lifted into the continuum, and the next two resonances to $v''=37$ becoming a quasibound level. For ${}^6\text{Li}-{}^7\text{Li}$, all three resonances are due to $v''=39$ being lifted into the continuum and becoming a quasibound level.

N''	v''	$\log_{10} E_{\text{res}}$ (a.u.)	Γ (a.u.)	τ (s)
${}^7\text{Li}_2$: $D_e=8516.75 \text{ cm}^{-1}$, $v''_{\max}=41$				
2	41	-7.64	2.35×10^{-9}	1.03×10^{-8}
3	41	-6.47	3.29×10^{-7}	7.36×10^{-11}
7	40	-5.70	5.84×10^{-8}	4.14×10^{-10}
${}^6\text{Li}_2$: $D_e=8516.70 \text{ cm}^{-1}$, $v''_{\max}=38$				
2	38	-6.88	1.36×10^{-7}	1.78×10^{-10}
6	37	-5.96	7.08×10^{-9}	3.42×10^{-9}
7	37	-5.47	5.01×10^{-7}	4.83×10^{-11}
${}^6\text{Li}-{}^7\text{Li}$: $D_e=8516.73 \text{ cm}^{-1}$, $v''_{\max}=39$				
4	39	-6.34	5.11×10^{-8}	4.73×10^{-10}
5	39	-5.84	6.93×10^{-7}	3.49×10^{-11}
6	39	-5.59	2.28×10^{-6}	1.06×10^{-11}

factor is maximal, and the classical turning points of the bound and continuum wave functions most nearly coincide. In Fig. 5, we sketch the turning points defined by the shape resonance; the inner wall turning point $R_1=6.383a_0$, and the inner and outer turning points of the centrifugal barrier are $R_2=37.52a_0$ and $R_3=45.90a_0$. The levels with the best overlap are $v'=2$ with the inner turning point located at $6.36a_0$, $v'=72$ with its outer turning point located at $37.89a_0$, and $v'=73$ with its outer turning point located at $47.15a_0$. The turning points of the surrounding levels are listed in Table II. We have calculated the intensities for v' up to 73, and we illustrate them in Fig. 6. Due to the rapid decrease of $D(R)$ at large R , the intensities are, with the exception of the $v'=1$ feature, all much less than the feature corresponding to $v'=2$, even for levels $v'=72$ and 73. The $v'=1$ feature is predicted to have an intensity equal to 77% of the $v'=2$ feature. Although $v'=1$ has not been populated in this experiment, it would be obscured by the high background signal [3].

We have searched numerically for shape resonances in the scattering by the interaction potentials of the $X^1\Sigma_g^+$ state of ${}^7\text{Li}_2$ and the $X^1\Sigma_g^+$ and $a^3\Sigma_u^+$ states of ${}^6\text{Li}{}^7\text{Li}$ and ${}^6\text{Li}_2$. For the $X^1\Sigma_g^+$ interaction potential, we adopted the curve described in Ref. [10]. The locations and widths of several of the resonances are listed in Tables III and IV. It may be possible to detect them experimentally. Accurate measurements could be used to improve the interaction potentials.

VI. DISCUSSION AND CONCLUSION

The feature measured in the spectrum of $2^3\Pi_g \rightarrow a^3\Sigma_u^+$ from the initial level $v'=2, N'=4$ corresponds to a shape resonance in the continuum of the $a^3\Sigma_u^+$ state. Its position of $2.5 \pm 0.2 \text{ cm}^{-1}$ above the last level $v''=9$ is in good agreement with the theoretical value of 2.4 cm^{-1} . Furthermore, the fact that the feature was seen only for one specific

transition is consistent with our calculations. Figure 7 shows the rotational energy levels of the $v''=9$ and 10 vibrational levels of the $a^3\Sigma_u^+$ state of ${}^7\text{Li}_2$. For $v''=10$, shape resonances appear above the dissociation threshold for $N''=4$ and 5, one of which we identify with the observed spectral feature.

The accuracy of the measurement does not allow an experimental determination of the width of the resonance. The uncertainty in the position of the resonance prevents us from using it to modify the inner wall of the $a^3\Sigma_u^+$ potential curve, which would make possible a more precise evaluation of the scattering length. A more precise determination of the position of the resonance is possible using a triple resonance spectroscopy where the fluorescence detection is replaced by stimulated emission pumping [16]. The laser frequency calibration accuracy is much higher than that of fluorescence-based methods. These experiments are planned at Temple University.

ACKNOWLEDGMENTS

The authors gratefully acknowledge helpful discussions with Dr. A.J. Ross. The Fourier Transform experiment in Lyon by Dr. A.J. Ross and co-workers supplied the calibration for the spectrum shown in this paper. We also thank Dr. Alexandra Yiannopoulos for her assistance with the experiment at Temple University, and for pointing out the correction in T_e . We also acknowledge G. Lazarov for technical assistance. The work of R.C. was supported by the National Science Foundation through a grant to the Institute for Theoretical Atomic and Molecular Physics (ITAMP), and of A.D. by the U.S. Department of Energy, Division of Chemical Sciences, Office of Energy Research. A.M. Lyyra gratefully acknowledges support from the National Science Foundation (Grant Nos. CHE-9222801 and CHE-9320110). Li Li thanks NNSF, China for support.

-
- [1] A. Yiannopoulou, K. Urbanski, S. Antonova, A. M. Lyyra, Li Li, T. An, T. J. Whang, B. Ji, X. T. Wang, W. C. Stwalley, T. Leininger, and G.-H. Jeung, *J. Chem. Phys.* **103**, 5898 (1995).
- [2] C. Linton, F. Martin, A. J. Ross, I. Russier, P. Crozet, A. Yiannopoulou, Li Li, and A. M. Lyyra, *J. Mol. Spectrosc.* **196**, 20 (1999).
- [3] A. M. Lyyra and A. J. Ross (private communication).
- [4] H. M. J. M. Boesten, C. C. Tsai, B. J. Verhaar, and D. J. Heinzen, *Phys. Rev. Lett.* **77**, 5194 (1996).
- [5] H. M. J. M. Boesten, C. C. Tsai, J. R. Gardner, D. J. Heinzen, and B. J. Verhaar, *Phys. Rev. A* **55**, 636 (1997).
- [6] R. H. G. Reid and A. Dalgarno, *Phys. Rev. Lett.* **22**, 1029 (1969).
- [7] H. M. J. M. Boesten, C. C. Tsai, D. J. Heinzen, A. J. Moonen, and B. J. Verhaar, *J. Phys. B* **32**, 287 (1999).
- [8] T. L. Stephens and A. Dalgarno, *J. Quant. Spectrosc. Radiat. Transf.* **12**, 569 (1972).
- [9] R. Côté and A. Dalgarno, *Phys. Rev. A* **58**, 498 (1998).
- [10] E. R. I. Abraham, W. I. McAlexander, J. M. Gerton, R. G. Hulet, R. Côté, and A. Dalgarno, *Phys. Rev. A* **55**, R3299 (1997).
- [11] M. Marinescu, *Phys. Rev. A* **56**, 4764 (1997).
- [12] This corrected value is derived from $T_e(\text{exp.}) = 29\,844.465\,3 \text{ cm}^{-1}$ in Ref. [1], where the sign of $Y_{00}(2^3\Pi_g) = -0.223\,2 \text{ cm}^{-1}$ was reversed, and $Y_{00}(X^1\Sigma_g^+) = -0.034\,49 \text{ cm}^{-1}$ from Ref. [13] omitted. Instead of $T_e = T_e(\text{exp.}) + Y_{00}(2^3\Pi_g) = 29\,844.242\,14 \text{ cm}^{-1}$ in Table II of Ref. [1], the correct value is $T_e = T_e(\text{exp.}) + Y_{00}(X^1\Sigma_g^+) - Y_{00}(2^3\Pi_g) = 29\,844.654\,01 \text{ cm}^{-1}$ [A. Yiannopoulou (private communication)].
- [13] M. M. Hessel and C. R. Vidal, *J. Chem. Phys.* **70**, 4439 (1979).
- [14] D. D. Konowalow and J. L. Fish, *Chem. Phys.* **84**, 463 (1984).
- [15] L. B. Ratcliff, J. L. Fish, and D. D. Konowalow, *J. Mol. Spectrosc.* **122**, 293 (1987).
- [16] A. M. Lyyra, H. Wang, T.-J. Whang, W. C. Stwalley, and L. Li, *Phys. Rev. Lett.* **66**, 2724 (1991).